Robust rhythmogenesis via spike-timing-dependent plasticity

Gabi Socolovsky [1,2,*] and Maoz Shamir [1,2,3]

[1]*Department of Physics, Faculty of Natural Sciences, Ben-Gurion University of the Negev, Be'er-Sheva 8410501, Israel*
[2]*Zlotowski Center for Neuroscience, Ben-Gurion University of the Negev, Be'er-Sheva 8410501, Israel*
[3]*Department of Physiology and Cell Biology, Faculty of Health Sciences, Ben-Gurion University of the Negev, Be'er-Sheva 8410501, Israel*

(Received 29 July 2020; revised 5 July 2021; accepted 21 July 2021; published 20 August 2021)

Rhythmic activity has been observed in numerous animal species ranging from insects to humans, and in relation to a wide range of cognitive tasks. Various experimental and theoretical studies have investigated rhythmic activity. The theoretical efforts have mainly been focused on the neuronal dynamics, under the assumption that network connectivity satisfies certain fine-tuning conditions required to generate oscillations. However, it remains unclear how this fine-tuning is achieved. Here we investigated the hypothesis that spike-timing-dependent plasticity (STDP) can provide the underlying mechanism for tuning synaptic connectivity to generate rhythmic activity. We addressed this question in a modeling study. We examined STDP dynamics in the framework of a network of excitatory and inhibitory neuronal populations that has been suggested to underlie the generation of oscillations in the gamma range. Mean-field Fokker-Planck equations for the synaptic weight dynamics are derived in the limit of slow learning. We drew on this approximation to determine which types of STDP rules drive the system to exhibit rhythmic activity, and we demonstrate how the parameters that characterize the plasticity rule govern the rhythmic activity. Finally, we propose a mechanism that can ensure the robustness of self-developing processes in general, and for rhythmogenesis in particular.

DOI: 10.1103/PhysRevE.104.024413

I. INTRODUCTION

Rhythmic activity in the brain has been observed for more than a century [1,2]. Oscillations in different frequency bands have been associated with different cognitive tasks and mental states [2–6]. Specifically, rhythmic activity in the gamma band has been described in association with sensory stimulation [7], attentional selection [8,9], working memory [10], and other measures [11]. Deviation from normal rhythmic activity has been associated with pathology [12–15].

Considerable theoretical efforts have been devoted to unraveling the neural mechanism responsible for generating rhythmic activity in general [2] and in the gamma band in particular [16–21]. One possible mechanism is based on delayed inhibitory feedback [21–24]. The basic architecture of this mechanism is composed of one excitatory and one inhibitory neuronal populations, with reciprocal connections Fig. 1(a). A target rhythm is obtained by tuning the strengths of the excitatory and inhibitory interactions [Figs. 1(b) and 1(c)]. However, it is unclear which mechanism results in the required fine-tuning [25,26].

We hypothesized that activity-dependent synaptic plasticity can provide the mechanism for tuning the interaction strengths in order to stabilize a specific rhythmic activity in the gamma band.

Here we focused on spike-timing-dependent plasticity (STDP) as the rhythmogenic process [25,26]. Below, we briefly describe STDP and derive the dynamics of the synaptic weights in the limit of slow learning. Since the cross-correlation of neural activity is central to STDP dynamics, we next define the network dynamics and analyze its phase diagram and the dependence of the correlations on the synaptic weights. Using the separation of timescales in the limit of slow learning, we analyze STDP dynamics and investigate under what conditions STDP can stabilize a specific rhythmic activity and how the characteristics of the STDP rule govern the resultant rhythmic activity. Finally, we summarize our results, discuss possible extensions and limitations, and propose a general principle for robust rhythmogenesis.

II. STDP DYNAMICS

The basic coin of information transfer in the central nervous system is the spike: a short electrical pulse that propagates along the axon (output branch) of the transmitting neuron to synaptic terminals that relay the information to the dendrites (input branch) of the receiving neurons downstream. While spikes are stereotypical, the relayed signal depends on the synaptic weight, which can be thought of as interaction strength. Learning is the process that modifies synaptic weights (the dynamics of the interaction strengths themselves), and typically occurs on a slower timescale than the timescale of the neuronal responses.

STDP is an empirically observed microscopic learning rule in which the modification of the synaptic weight depends on the temporal relation between the spike times of the pre- (transmitting) and post- (receiving) synaptic neurons [27–31]. Following [32], the change, ΔJ_{ij}, in the synaptic weight J_{ij} from the presynaptic neuron j to the postsynaptic neuron i is

*gabisoco@post.bgu.ac.il

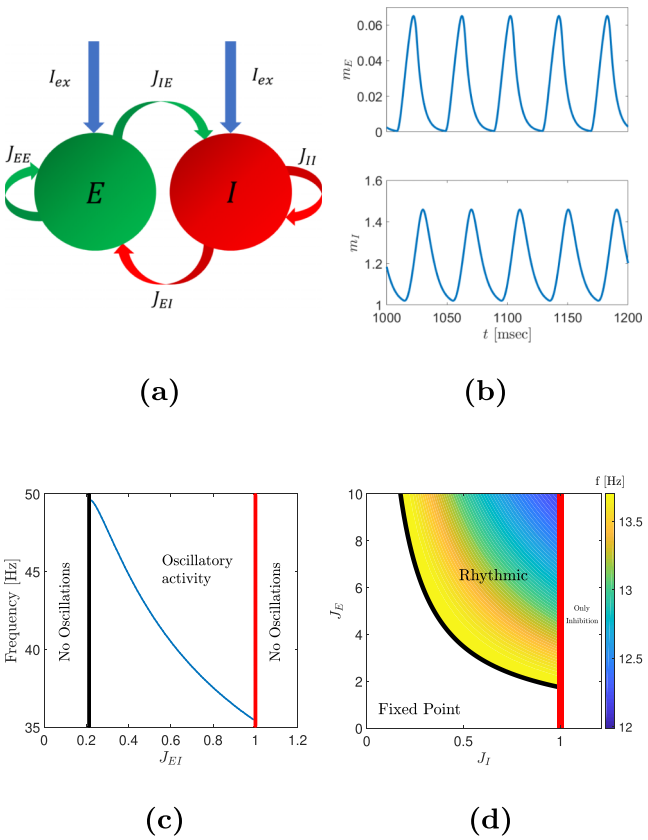

FIG. 1. The excitatory-inhibitory network. (a) Model architecture. The neuronal network here is composed of an excitatory (E) and an inhibitory (I) populations with inter- (J_{IE} and J_{EI}) and intra- (J_{II} and J_{EE}, which will be taken to zero hereafter) connections. The interaction is not symmetric and is delayed. (b) The oscillatory dynamics of the mean excitatory and inhibitory population firing rates m_E and m_I, respectively, at a frequency of 24.9 Hz. Here we used $J_{EE} = J_{II} = 0$, $J_{IE} = 8.91$, $J_{EI} = 0.9$, and $\tau_m = d = 5$ ms [see Eqs. (7) and (8) below]. (c) Rhythmic activity. The oscillation frequency is depicted as a function of the strength of the inhibitory to excitatory connection, J_{EI}. The following parameters were implemented here: $J_{EE} = J_{II} = 0$, $J_{IE} = 50$, $\tau_m = 10$ ms, and $d = 1$ ms. (d) Phase diagram of the delayed rate model. Strong inhibition, $J_I > 1$, leads the system to a purely inhibitory fixed point, in which m_E is fully suppressed and $m_I = 1$. For weak to moderate inhibition, $J_I \in (0, 1)$, and below the black line, the system converges to a fixed point, where both populations are active. For $\bar{J} > \bar{J}_d$ (above the black line) the model exhibits rhythmic activity. For a given time delay, the frequency is governed by $\bar{J}$. When $\bar{J}$ is decreased, higher frequencies are observed. Here we used $\tau_m = d = 1$.

expressed as the sum of two processes: potentiation (i.e., increasing the synaptic weight) and depression (i.e., decreasing the synaptic weight):

$$\Delta J_{ij} = \lambda[K_+(\Delta) - \alpha K_-(\Delta)], \tag{1}$$

where $\Delta = t_i - t_j$ is the pre- and postspike time difference. Functions $K_\pm(\Delta) \geqslant 0$ describe the temporal structure of the potentiation (+) and depression (−) of the STDP rule. Parameter α denotes the relative strength of the depression, and λ is the learning rate. We assume that learning occurs on a slower timescale than the characteristic timescales that describe neuronal activity (for given fixed synaptic weights).

A wide range of temporal structures of STDP rules has been reported [33–40]. Here we focus on two families of rules. One is composed of temporally symmetric rules and the other is made up of temporally asymmetric rules.

For the temporally symmetric family, we apply a difference of Gaussian STDP rule, namely

$$K_\pm(t) = \frac{1}{\sqrt{2\pi}\,\tau_\pm} e^{-(t/\tau_\pm)^2/2}, \tag{2}$$

where $\tau_\pm$ denotes the characteristic timescales of the potentiation (+) and depression (−). Consistent with the popular description of the famous Hebb rule that "neurons that fire together wire together" [41], we refer to the case of $\tau_+ < \tau_-$ as Hebbian, and $\tau_+ > \tau_-$ as anti-Hebbian.

For the temporally asymmetric STDP rules, we take

$$K_\pm(t) = \frac{1}{\tau_\pm} e^{\mp Ht/\tau_\pm} \Theta(\pm Ht), \tag{3}$$

where $\Theta(x)$ is the Heaviside step function, $\tau_\pm$ are the characteristic timescales of the potentiation (+) and depression (−), and $H = \pm 1$ dictates the Hebbianity of the STDP rule. The rule will be termed Hebbian for $H = 1$ when potentiation occurs in the causal branch, $t_{\text{post}} > t_{\text{pre}}$, and anti-Hebbian for $H = -1$.

Different types of synapses have been reported to exhibit different types of STDP rules. Consequently, there is no *a priori* reason to assume that excitatory and inhibitory synapses share the exact same learning rule. In particular, the characteristic time constants $\tau_{E,\pm}$ for excitatory synapses and $\tau_{I,\pm}$ for inhibitory synapses may differ.

Changes to synaptic weights due to the plasticity rule of Eq. (1) at short time intervals occur as a result of either a pre- or postsynaptic spike during this interval. Thus,

$$\begin{aligned}\dot{J}_{ij}(t) = {} & \lambda\rho_i(t)\int_0^\infty \rho_j(t-t')[K_+(t') - \alpha K_-(t')]dt' \\ & + \lambda\rho_j(t)\int_0^\infty \rho_i(t-t')[K_+(-t') - \alpha K_-(-t')]dt',\end{aligned} \tag{4}$$

where $\rho_{\text{post/pre}}(t) = \sum_l \delta(t - t_l^{\text{post/pre}})$ is the spike train of the post/pre neuron written as the sum of the δ function at the neuron's spike times $\{t_l^{\text{post/pre}}\}_l$. In the limit of slow learning, $\lambda \to 0$, the right-hand side of Eq. (4) can be replaced by its temporal mean (see [32] for complete derivations). This approximation has been termed the mean-field Fokker-Planck approximation [28]. As fluctuations vanish in this limit and deterministic dynamics are retained for the mean synaptic weights, we get

$$\dot{J}_{ij}(t) = \lambda\int_{-\infty}^{\infty} \Gamma_{ij}(-t')[K_+(t') - \alpha K_-(t')]dt', \tag{5}$$

where $\Gamma_{ij}(t)$ is the cross correlation of neurons i and j:

$$\Gamma_{ij}(t) = \langle \rho_i(t')\rho_j(t'+t)\rangle. \tag{6}$$

The angular brackets $\langle\cdots\rangle$ denote ensemble averaging over the neural noise and temporal averaging over one period in the

case of rhythmic activity (see [25,32] for more details). Note that the dependence of the right-hand side of Eq. (5) on time, t, occurs through the dependence of the cross-correlations on the synaptic weights at time t. Thus, the key to analyzing STDP dynamics is the ability to compute the cross-correlations of the neural activities and grasp their dependence on the synaptic weights. To this end, we examined rhythmogenesis in the gamma band using the framework of a reduced rate model with delay, proposed by Roxin and colleagues [Fig. 1(a)]. A complete analysis of the model appears in [21–23]. Below, we briefly describe the phase diagram of the system and derive the cross-correlations.

III. THE DELAYED EXCITATORY INHIBITORY NETWORK

The firing of different neurons is assumed to follow independent inhomogeneous Poisson process statistics with instantaneous firing rates that adhere to the reduced model in Roxin *et al.* [21]. In their work, Roxin and colleagues considered a full model that included inter-population as well as intrapopulation interactions (i.e., excitatory-excitatory and inhibitory-inhibitory). Here, for simplicity, we restrict the analysis to the minimal model that can reproduce oscillations in the gamma band. To do so, we model the rate dynamics of the gamma generating network by

$$\tau_m \dot{m}_E(t) = -m_E(t) + [I - J_I m_I(t-d)]_+, \tag{7}$$

$$\tau_m \dot{m}_I(t) = -m_I(t) + [I + J_E m_E(t-d)]_+, \tag{8}$$

where $m_{E/I}(t)$ is the mean firing rate of the excitatory (E) and inhibitory (I) population at time t. τ_m is the neuronal time constant. Unless stated otherwise, we take $\tau_m = 1$, which is equivalent to measuring time in units of the neuronal time constant. Parameter d denotes the delay, I is the external input to the system, and $[x]_+ = x$ for $x > 0$ and zero otherwise is taken to be the neuronal transfer function. In our analysis, we took $I = 1$. J_E and J_I are the effective interaction strengths between the two populations. J_E (J_I) can be thought of as a global order parameter reflecting the mean synaptic weight from the excitatory (inhibitory) presynaptic population to the inhibitory (excitatory) postsynaptic population.

For strong inhibition, $J_I > 1$, the system converges to a fixed point in which the excitatory population is fully suppressed by the inhibitory population, $\vec{m}^* = \binom{0}{1}$. For weak to moderate levels of inhibition, $J_I \in (0, 1)$, the system has a fixed point in which both populations are active, $\vec{m}^* \equiv \binom{m_E^*}{m_I^*} = \frac{1}{1+\bar{J}^2}\binom{1-J_I}{1+J_E}$, with $\bar{J} \equiv \sqrt{J_E J_I}$. However, this fixed point is not stable for $\bar{J} > \bar{J}_d$, where $\bar{J}_d^2 = 1 + \omega_d^2$, $\omega_d = \cot(\omega_d d)$, and $\omega_d \in [0, \pi/2d]$ (see Roxin *et al.* [21]). In this region ($\bar{J} > \bar{J}_d$ and $J_I < 1$), the system converges to a limit cycle solution, Fig. 1(d).

By rescaling the firing rates, the two-dimensional first-order delayed dynamics, Eqs. (7) and (8), can be reduced to a one-dimensional delayed dynamic equation:

$$\ddot{x}(t) + 2\dot{x}(t) + x(t) - [1 - \bar{J}^2 x(t-2d)]_+ = 0, \tag{9}$$

with

$$m_I(t) = 1 + (J_E - \bar{J}^2)x(t), \tag{10}$$

$$m_E(t-d) = \frac{J_E - \bar{J}^2}{J_E}[x(t) + \dot{x}(t)]. \tag{11}$$

Equation (9) highlights the fact that the temporal structure of the limit-cycle solution depends on the synaptic weights, J_E and J_I, only via $\bar{J}$. In particular, the period of oscillations is solely a function of $\bar{J}$ and d. As shown in Fig. 2(a), the period is a monotonically increasing function of both $\bar{J}$ and d.

In our model, the cross-correlations are given by temporal averaging of the mean firing rates, $\Gamma_{IE}(\Delta) \equiv \langle m_I(t) m_E(t+\Delta)\rangle$. In the fixed-point region of the phase diagram, the cross-correlation is simply given by the product of the mean rates, $\Gamma_{IE}(\Delta) = (1 - J_I)(1 + J_E)/(1 + \bar{J}^2)^2$.

In the region of the phase diagram where the system converges to a limit-cycle solution, Eqs. (10) and (11) provide the scaling of the cross-correlations, namely

$$\Gamma_{IE}(\Delta) = a\bar{x} + b\left(\Gamma_x(\Delta + d) + \frac{d}{d\Delta}\Gamma_x(\Delta + d)\right), \tag{12}$$

where $a \equiv (J_E - \bar{J}^2)/J_E$, $b \equiv (J_E - \bar{J}^2)^2/J_E$, $\bar{x} \equiv \langle x(t)\rangle$, and $\Gamma_x(s) \equiv \langle x(t)x(t+s)\rangle$. Note that $\bar{x}$ and Γ_x depend solely on the delay, d, and $\bar{J}$. Numerical investigation reveals that the autocorrelation of $x(t)$ is well approximated by a cosine function,

$$\Gamma_x(s) \approx \bar{\Gamma}_x + \tilde{\Gamma}_x \cos(\omega s), \tag{13}$$

where we used

$$\bar{\Gamma}_x = \int_0^T \Gamma_x(s) ds/T, \tag{14}$$

$$\tilde{\Gamma}_x = 2\int_0^T \Gamma_x(s)\cos(2\pi s/T) ds/T, \tag{15}$$

with T denoting the period of the limit cycle, as can be seen from the value of R^2, Fig. 2(b). The goodness of fit of the cosine approximation decreases when $\bar{J}$ or d is increased. Nevertheless, for a wide range of parameters relevant to the generation of gamma oscillations, R^2 is extremely high [$R^2 > 0.98$ throughout Fig. 2(b)]. Both $\bar{x}$ and $\bar{\Gamma}_x$ monotonically decrease as $\bar{J}$ increases, Figs. 2(c) and 2(d). In addition, they transition the bifurcation line continuously. On the other hand, $\tilde{\Gamma}_x$ does not transition in a continuous manner: it is zero in the fixed-point region and jumps to a positive value in the rhythmic region, Fig. 2(e).

Using the cosine approximation for the correlations, Eq. (13) and the scaling Eqs. (10) and (11) yield the semiempirical excitatory-inhibitory cross-correlations function:

$$\Gamma_{IE}(\Delta) \approx \bar{\Gamma} + \tilde{\Gamma}\cos(\omega\Delta + \tilde{\varphi}) \tag{16}$$

with $\bar{\Gamma} = a\bar{x} + b\bar{\Gamma}_x$, $\tilde{\Gamma} = b\tilde{\Gamma}_x(1+\omega^2)^{1/2}$, $\tilde{\varphi} = \omega(d + \varphi_\omega)$, and $\omega\varphi_\omega = \arcsin(\omega/\sqrt{1+\omega^2})$. Figure 3 shows the values of $\tilde{\varphi}$ on the phase diagram. The phase $\tilde{\varphi}(\bar{J}, d)$ is $\pi/2$ on the bifurcation line and weakly decreases as $\bar{J}$ is further increased. Note that $\Gamma_{EI}(\Delta) = \Gamma_{IE}(-\Delta)$.

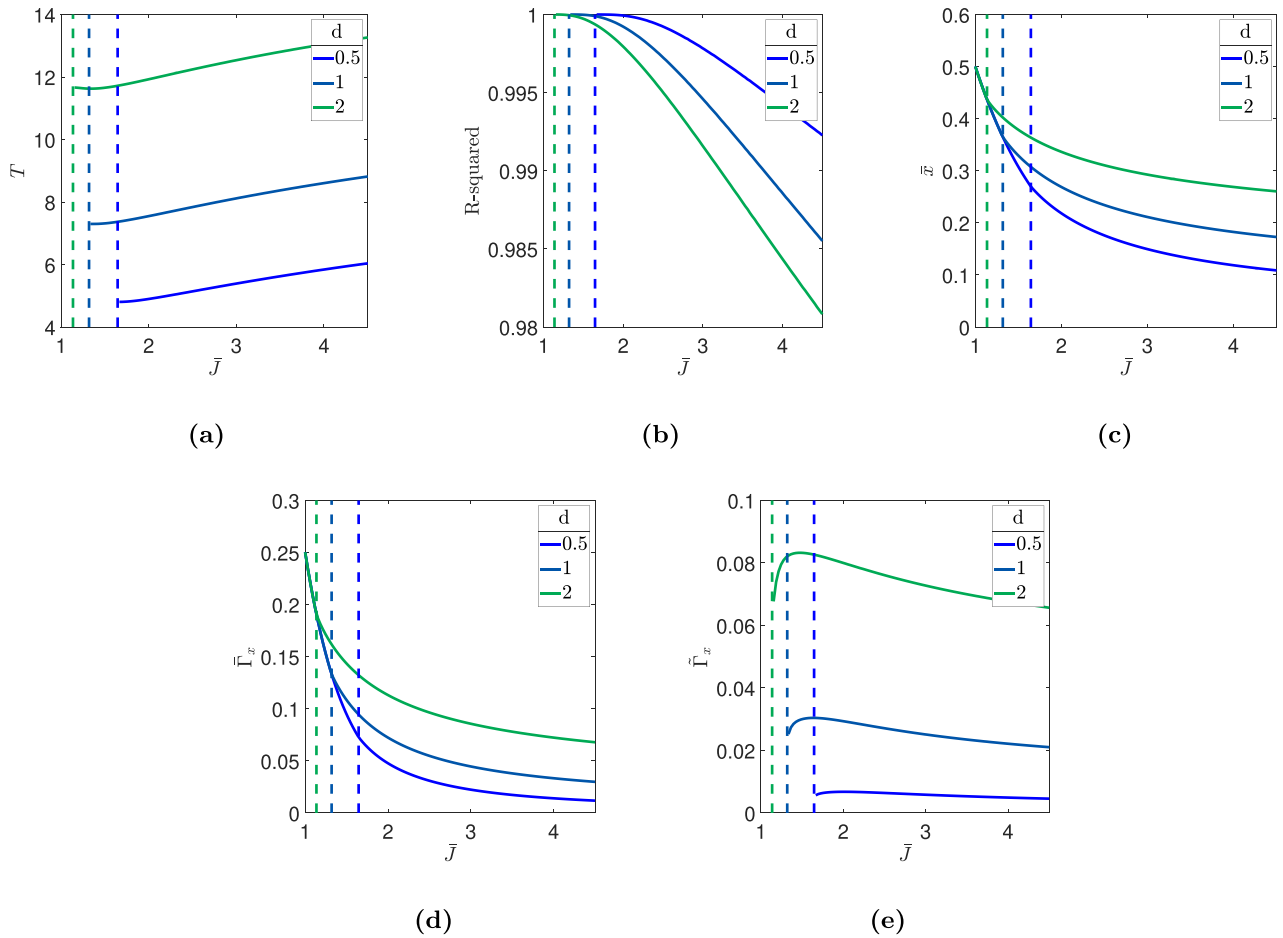

FIG. 2. Dynamics of the one-dimensional variable x, Eq. (9). Different features characterizing the dynamics of x are shown as a function of $\bar{J}$ for different values of the delay, d, differentiated by color. The dashed lines indicate the values of $\bar{J}_d$ for different delays, shown by color. The parameters plotted are as follows: (a) The period of the oscillations. (b) The goodness of fit of the cosine approximation, Eq. (13), of Γ_x, R^2. (c) The temporal average of x, $\bar{x}$. (d) The zeroth-order Fourier component of the autocorrelation of x, $\bar{\Gamma}_x$. (e) The first-order Fourier component of the autocorrelation of x, $\tilde{\Gamma}_x$.

IV. STDP INDUCED FLOW ON THE PHASE DIAGRAM

Utilizing the semiempirical cross-correlations, Eq. (16), yields the following dynamics for the synaptic weights:

$$\dot{J}_\sigma = \lambda(\bar{\Gamma}\bar{K} + \tilde{\Gamma}\tilde{K}_\sigma), \tag{17}$$

where

$$\bar{K} = \int_{-\infty}^{\infty} K(\Delta) d\Delta, \tag{18}$$

$$\tilde{K}_\sigma \equiv \int_{-\infty}^{\infty} K(\Delta)\cos(\omega\Delta_\sigma + \tilde{\varphi}) d\Delta, \tag{19}$$

where $\sigma = E, I$. We used the notation $K(\Delta) = K_+(\Delta) - \alpha K_-(\Delta)$ and $\Delta_E = -\Delta$, whereas $\Delta_I = \Delta$.

The STDP dynamics, Eq. (17), induces a flow in the phase plane of the synaptic weights $[J_I, J_E]$, which is also the phase diagram of the neural responses. The right-hand side of Eq. (17) depends on the synaptic weights through the Fourier transforms of the cross-correlations $\bar{\Gamma}$ and $\tilde{\Gamma}$. Using the separation of timescales between the fast neuronal responses and the slow learning rate, in the limit of slow learning $\lambda \to 0$, one can compute $\bar{\Gamma}$ and $\tilde{\Gamma}$ from the neuronal dynamics for fixed synaptic weights.

Thus, STDP induces a flow on the phase diagram of the system. Rhythmogenesis is obtained when this flow guides the system and stabilizes it at a fixed point on the phase diagram that is characterized by the desired rhythm.

In the region of the phase diagram in which the mean neuronal firings relax to a fixed point, $\tilde{\Gamma} = 0$. Due to our choice of normalization, $\bar{K}_\pm = 1$, in this region $\mathrm{sgn}(\dot{J}_\sigma) = \mathrm{sgn}(1 - \alpha_\sigma)$, $\sigma \in \{E, I\}$. Consequently, the STDP dynamics will induce a flow from the fixed-point region towards the rhythmic region if and only if the potentiation is strong relative to the depression for both types of synapses, $\alpha_E, \alpha_I < 1$ (except for a small region of the phase diagram with high inhibition and low excitation, which also depends on the learning rates, λ_E and λ_I, of the different synapses). This result holds true for any STDP rule. In contrast, the STDP dynamics in the rhythmic region of the phase diagram depend on the temporal structure of the learning rule.

The difference of Gaussians learning rule, Eq. (2), yields

$$\tilde{K}_\sigma = \cos\tilde{\varphi}\left(e^{-\frac{(\omega\tau_{\sigma,+})^2}{2}} - \alpha e^{-\frac{(\omega\tau_{\sigma,-})^2}{2}}\right), \tag{20}$$

with $\sigma \in \{E, I\}$. Consequently, the dynamical equations of J_E and J_I will be identical if the characteristic timescales of

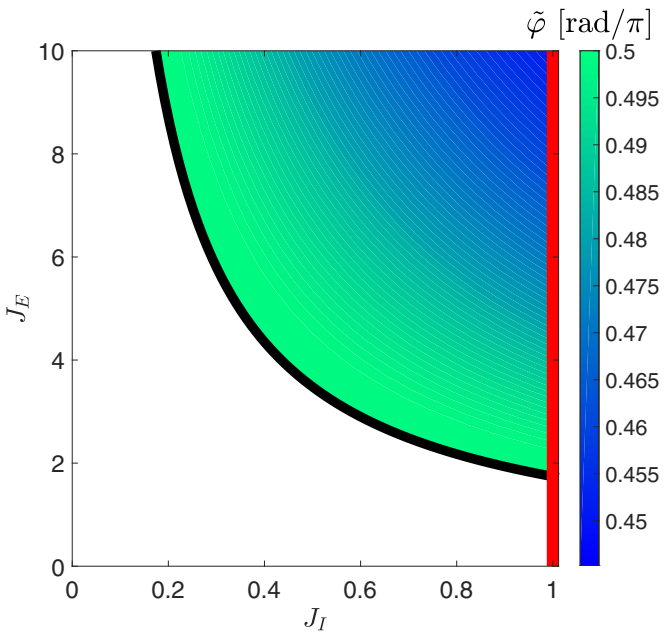

FIG. 3. The values of $\tilde{\varphi}$. The parameter $\tilde{\varphi}/\pi$ is shown by color as a function of J_E and J_I on the phase diagram. Here $d = 1$ was used.

potentiation and depression are the same, i.e., if $\tau_{E,+} = \tau_{I,+}$ and $\tau_{E,-} = \tau_{I,-}$. Note that on the right-hand side of Eq. (20), the term $\cos\tilde{\varphi}$ ensures that $\tilde{K}_\sigma$ is zero on the bifurcation (see Fig. 3). Figures 4(a) and 4(b) depict the nullclines of J_E and J_I, respectively, for different values of the relative strength of depression, α [in (a)], and the characteristic time of depression, τ_- [in (b)], differentiated by color. We show that for $\alpha < 1$ ($\alpha > 1$) and $\tau_+ > \tau_-$ ($\tau_+ < \tau_-$) the nullcline of J_E and the left branch of the nullcline of J_I are stable (unstable). A fixed point of the STDP dynamics is obtained by the intersection of J_E and J_I nullclines. For the difference of Gaussians rule, a stable fixed point that exhibits rhythmic activity in the gamma band can thus be obtained. However, this requires a delicate adjustment of the parameters characterizing the STDP learning rules.

For the temporally asymmetric Hebbian exponential rule, Eq. (3) with $H = 1$, we obtain

$$\begin{aligned}\tilde{K}_\sigma = &\cos(\theta_{\sigma,+})\cos(\theta_{\sigma,+} - \tilde{\varphi}_\sigma) \\ &- \alpha\cos(\theta_{\sigma,-})\cos(\theta_{\sigma,-} + \tilde{\varphi}_\sigma),\end{aligned} \tag{21}$$

where $\cos(\theta_{\sigma,\pm}) = [1 + (\omega\tau_{\sigma,\pm})^2]^{-1/2}$, $\tilde{\varphi}_E = \tilde{\varphi}$, and $\tilde{\varphi}_I = -\tilde{\varphi}$. Now, due to $\theta_{\sigma,\pm}$, the term $\tilde{\Gamma}\tilde{K}_\sigma$ transitions discontinuously across the bifurcation line, thus inducing discontinuity in $\dot{J}_E$ and $\dot{J}_I$ along the transition from the fixed point to the rhythmic region. Figures 4(c) and 4(d) depict the nullclines of J_I for the temporally asymmetric Hebbian learning rule for different values of the relative strength of depression, α [in (c)], and the characteristic time of depression, τ_- [in (d)], differentiated by color. The left branch of the nullclines of J_I is stable (unstable) for $\alpha < 1$ ($\alpha > 1$) and $\tau_+ < \tau_-$ ($\tau_+ > \tau_-$). Interestingly, a considerable part of the J_I nullcline is on the bifurcation line.

For the temporally asymmetric Hebbian learning rule, the dynamics of J_E do not have a nullcline. As a result, a fixed point does not exist, and the temporally asymmetric Hebbian STDP rule cannot stabilize rhythmic activity in the gamma range.

However, as $\Gamma_{EI}(\Delta) = \Gamma_{IE}(-\Delta)$, the temporally asymmetric *anti*-Hebbian exponential rule [Eq. (3) with $H = -1$] for excitatory synapses, J_E, in our model, defines the exact same dynamics as that of inhibitory synapses, J_I, with a Hebbian rule [Eq. (3) with $H = +1$]. Therefore, an asymmetric Hebbian learning rule for J_I and an asymmetric anti-Hebbian learning rule for J_E yield the same nullclines [see Figs. 4(c) and 4(d)]. Moreover, because a considerable part of the nullcline is on the bifurcation line, no fine-tuning of the parameters is required to obtain a fixed point of the STDP dynamics that will generate rhythmic activity at ω_d. Thus, the STDP dynamics have a line attractor on (part of) the bifurcation line. Furthermore, when the left branches of the nullclines of J_E and J_I are stable ($\alpha < 1$, $\tau_{E,-} > \tau_{E,+}$, and $\tau_{I,-} > \tau_{I,+}$) and the nullcline of J_I departs from the bifurcation line below the nullcline of J_E, the attractor line is stable against perturbations in every direction [see Fig. 4(e)].

V. DISCUSSION

Previous studies have investigated the effects of rhythmic activity on STDP [20,42–51]. However, in these studies, rhythmic activity was hard-wired in the system, and the issue of rhythmogenesis was not addressed.

Rhythmogenesis can be thought of as self-organizing temporal activity, i.e., the ability of a nonrhythmic system to spontaneously develop rhythmic activity. In our approach, the process of rhythmogenesis was mapped to a flow on the phase diagram. This mapping relies on the separation of timescales.

Previously, Soloduchin and Shamir investigated rhythmogenesis using the framework of two neuronal populations with reciprocal inhibition and short-term adaptation in the form of firing rate adaptation [25,26]. The network motif of reciprocal inhibition has been widely reported in the central nervous system [52–54]. However, it is mainly associated with winner-take-all-like competition [55–61] rather than generating rhythmic activity (but see [62,63] on the spinal cord). Here, rhythmogenesis was studied in the framework of a network that is considered a valid hypothesis for generating gamma rhythm in the brain [21–23].

In Soloduchin and Shamir [25], rhythmogenesis was obtained as a specific stable fixed point on the phase diagram of the system, in which due to the temporal characteristics of the STDP rule, the dynamics of the synaptic weights vanish at a specific frequency. This scenario is similar to the case of temporally symmetric STDP [Figs. 4(a) and 4(b)]. However, scientifically this scenario is somewhat disappointing, since we have traded the problem of fine-tuning of the synaptic weights for the problem of fine-tuning of the characteristics of the STDP rule [26].

The temporally asymmetric STDP rule provides a possible solution to the fine-tuning problem of rhythmogenesis, which we term *critical rhythmogenesis* [Figs. 4(c)–4(e)]. Rhythmogenesis in the temporally asymmetric STDP rule is not obtained as a fixed point of the STDP dynamics. Rather, in this case, rhythmogenesis utilizes the discontinuity of $\tilde{\Gamma}$ across the bifurcation line. For a wide range of parameters, the flow

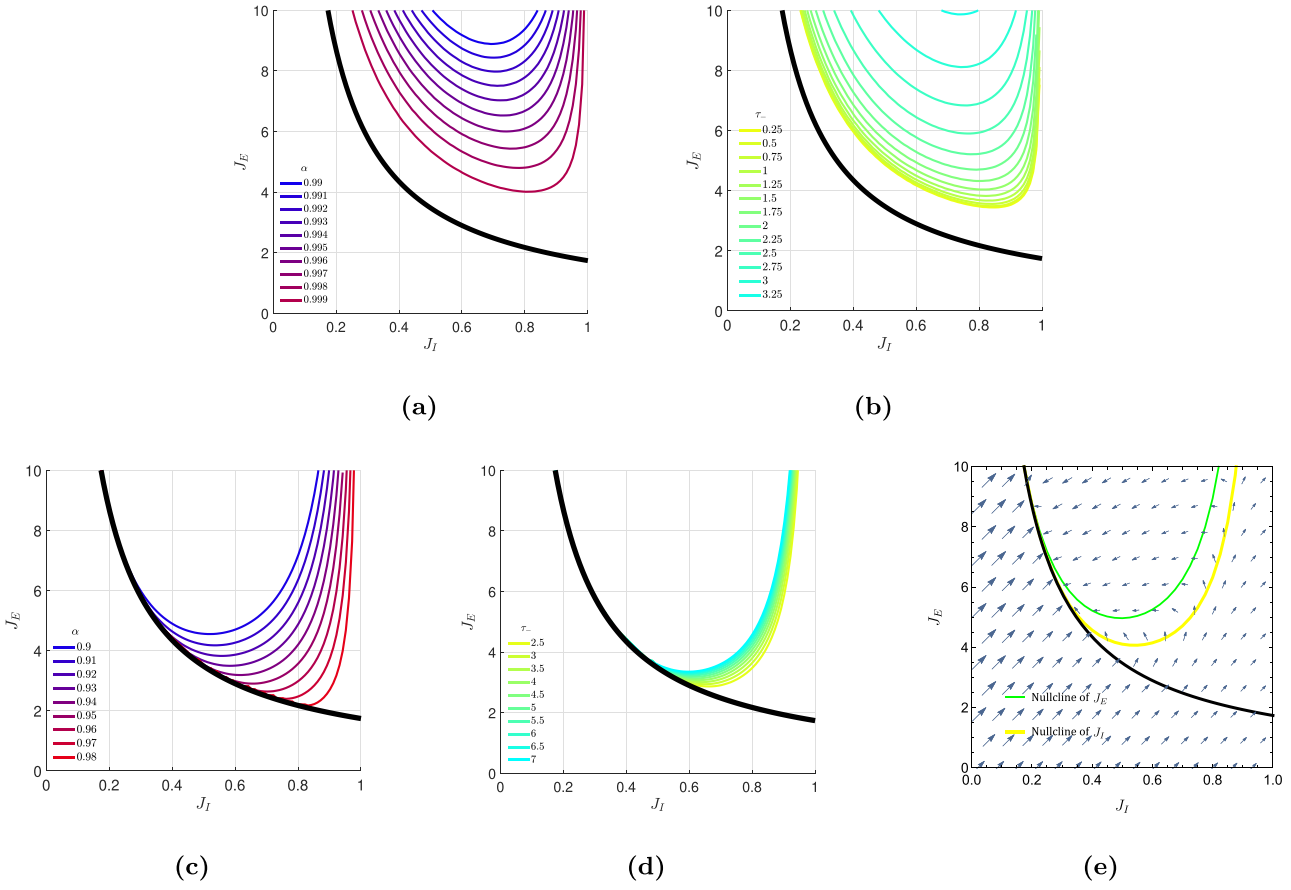

FIG. 4. Nullclines of the STDP dynamics. (a),(b) The nullclines of J_E and J_I for the difference of Gaussians learning rule (in this case, the nullclines are identical for the same choice of parameters α, $\tau_\pm$) The nullclines are shown for different values of $\alpha = 0.99, 0.991, \ldots, 0.999$, differentiated by color, with $\tau_+ = 2$ and $\tau_- = 1$, in (a). The nullclines are shown for different values of $\tau_- = 0.25, 0.5, \ldots, 3.25$, by colors, with $\tau_+ = 5$ and $\alpha = 0.999$, in (a). (c),(d) The nullclines of J_I (J_E) for the temporally asymmetric Hebbian (anti-Hebbian) STDP rule. The nullclines are shown for different values of $\alpha = 0.9, 0.91, ...0.99$, with $\tau_+ = 2$ and $\tau_- = 5$, in (c). The nullclines are shown for different values of $\tau_- = 2.5, 3, \ldots, 7$, with $\tau_+ = 2$ and $\alpha = 0.94$, in (d). The nullclines were computed using the cosine approximation for the neuronal cross-correlations. (e) The vector flow in the case of a temporally asymmetric Hebbian learning rule for J_I and a temporally asymmetric anti-Hebbian learning rule for J_E. The nullclines are shown for $\alpha = 0.88$, $\tau_{I,+} = \tau_{E,+} = 1$, $\tau_{I,-} = 2$, and $\tau_{E,-} = 5$. The learning rates are $\lambda_I = 1$ and $\lambda_E = 10$. In every subfigure, $d = 1$ was used.

induced by the STDP is directed from the fixed-point region towards the rhythmic region and from the rhythmic region to the fixed-point region, and the system will settle on the bifurcation line itself. Consequently, the resultant rhythmic activity will be dictated by bifurcation (e.g., the firing rates will oscillate at ω_d), which is independent of the synaptic plasticity, thus accounting for the robustness to the parameters that characterize the STDP.

Figure 5(a) presents an illustration of critical rhythmogenesis with finite learning rate, $\lambda > 0$. As can be seen from the figure, for relatively strong potentiation, $\alpha < 1$, the STDP dynamics draws the system towards the rhythmic region. The noise in the dynamics results from the spiking activity of the neurons that follows an inhomogeneous Poisson process with rates given by Eqs. (7) and (8). Note that due to the discontinuity [of $\tilde{\Gamma}_x$, cf. Fig. 2(e)] across the bifurcation, the STDP dynamics pulls the system towards the bifurcation line from both sides, but it does not vanish on it. Consequently, the system can drift along the bifurcation line. This drift can be restricted by suppressing the potentiation when the synaptic weight becomes too strong, as done in, e.g., [28,32,64]; see Fig. 5(b).

The discontinuity of $\tilde{\Gamma}_x$ across the bifurcation line results from a degenerate Hopf bifurcation that can be traced to the choice of a threshold linear transfer function, e.g., Eq. (7). Indeed, on the bifurcation line itself, one can show that the degenerate solutions are sinusoidal functions of time around the fixed-point solution with angular velocity of w_d and any arbitrary amplitude that is less than $\sqrt{2\Delta\tilde{\Gamma}_x}$, where $\Delta\tilde{\Gamma}_x$ is the discontinuity in $\tilde{\Gamma}_x$ across the transition (specifically, $\Delta\tilde{\Gamma}_x = \frac{1}{2[\bar{J}_d^2(1+\bar{J}_d^2)]^2}$). Roxin and Montbrió, in an elegant study, investigated the effect of a smooth transfer function in a related model [24]. Their analysis provided a criterion that determines, based on the transfer function and its derivatives, whether the bifurcation will be subcritical or supercritical. In particular, their investigation showed that the frequently used logistic function may only yield supercritical bifurcation in their model, thus eliminating the discontinuity across the transition.

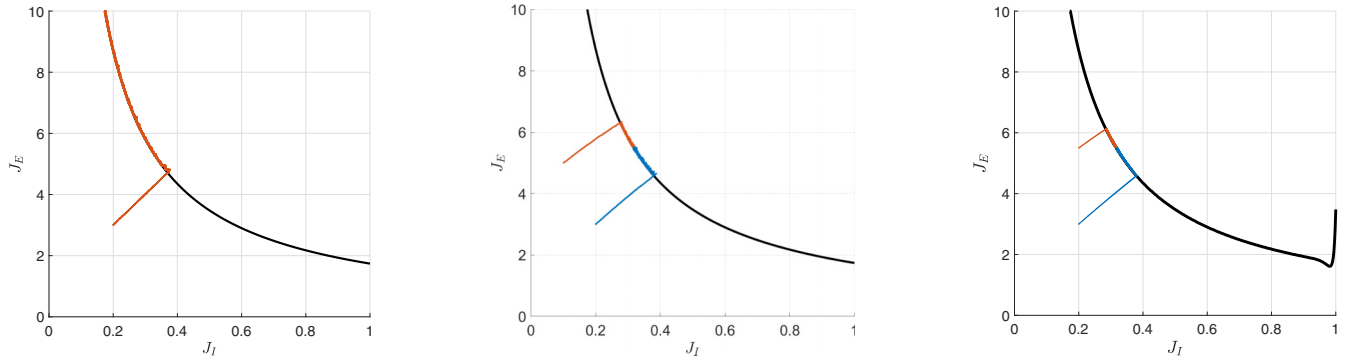

FIG. 5. Critical rhythmogenesis. (a) STDP dynamics at finite learning rate. Equation (4) was solved numerically with $\lambda_E = 10 \times \lambda_I = 0.0004$, where the spike times of the excitatory and inhibitory neurons obeyed an inhomogeneous Poisson process with mean rates given by Eqs. (7) and (8); see Appendix 1 for details. The red trace depicts the trajectory of the synaptic weights on the phase diagram of the system in the plane of $[J_I, J_E]$. (b) STDP dynamics at finite $\lambda_E = 10 \times \lambda_I = 0.0004$ and suppression of potentiation. STDP dynamics with a modified learning rule, Eq. (A1) (see Appendix 2 for details), was solved numerically. The red and blue traces show the trajectories of the synaptic weights for different initial condition. (c) STDP dynamics with a smooth transfer function, Eq. (A3); see Appendix 3 for details. In all of the above figures, the bifurcation line is shown for reference (black). In all simulations, we used the temporally asymmetric Hebbian (anti-Hebbian) exponential kernel, Eq. (3), for the inhibitory (excitatory) synapses with $\tau_{E,+} = \tau_{I,+} = 1$, $\tau_{I,-} = 2$, $\tau_{E,-} = 5$, $\alpha = 0.9$, a delay of $d = 1$, and $\tau_m = 1$.

Figure 5(c) depicts the STDP dynamics for a model with a smooth transfer function (see Appendix 3 for details). As can be observed, the phase diagram has been modified somewhat. Nevertheless, qualitatively similar results are still obtained. Namely, the STDP dynamics draws the system towards the bifurcation line, along which it may drift. This drift can be limited by adding weight dependence to the STDP learning rule that suppresses potentiation for strong synapses.

Recently, Pernelle and colleagues studied the possible contribution of gap junction plasticity to rhythmic activity [65]. They postulated a plasticity rule for gap junctions that tuned the system to operate on the boundary of asynchronous regular firing activity on the one hand, and rhythmic activity of synchronous bursts on the other. In the context of our work, this can be viewed as an example of critical rhythmogenesis, which explains the robustness of their putative mechanism to variations in the plasticity rule.

We suggest that the scenario of critical rhythmogenesis may provide a general principle for robustness in biological systems. Assume that a certain biological system, which is characterized by set parameters $\{x_1, x_2, \ldots, x_n\}$ (i.e., $\vec{x}$ is a point in the phase diagram of the system), is required to maintain a certain living condition, $f(\{x_1, x_2, \ldots, x_n\}) = 0$. This condition is met by a homeostatic process. The homeostatic process defines the dynamics on $\{x_1, x_2, \ldots, x_n\}$, which are characterized by another set of parameters, $\{\alpha_1, \alpha_2, \ldots, \alpha_m\}$, namely $\dot{\vec{x}} = \mathcal{F}(\vec{x}, \vec{\alpha})$. A viable homeostatic process is a choice of parameters, $\vec{\alpha}^*$, such that the homeostatic dynamics will lead the system to a set of parameters, x_∞, that satisfy the living condition, $f(\vec{x}_\infty) = 0$.

How can this be achieved? One possibility is that x_∞ is a stable fixed point of the homeostatic dynamics, in which $\mathcal{F}(\vec{x}_\infty, \vec{\alpha}^*) = 0$. This solution requires fine-tuning of the parameters that define the homeostatic process, $\vec{\alpha}$. In this case, fluctuations in $\vec{\alpha}$ will generate fluctuations in $\vec{x}$ away from x_∞.

An alternative scenario is that the homeostatic dynamics utilize some discontinuity in the phase diagram. In this scenario, the dynamics do not necessarily vanish on x_∞, $\mathcal{F}(\vec{x}_\infty, \vec{\alpha}^*) \neq 0$. Rather, due to the discontinuity there exists a wide range of parameters, $\{\alpha_1, \alpha_2, \ldots, \alpha_m\}$, such that the dynamics draw the system towards the discontinuity from both sides, as is the case for critical rhythmogenesis. Consequently, this scenario can stabilize the system in a critical condition on the boundary of two phases.

The idea that the central nervous system may operate in (or near) a critical condition has been suggested in the past, and it may have computational advantages [66–68]. However, this latter scenario also has shortcomings. The most obvious is that it can only be used to ensure and stabilize critical behavior. In addition, it cannot be used when one of the phases near the critical line is lethal.

An advantage of critical rhythmogenesis is that it allows for rapid switching between rhythmic and nonrhythmic phases, for example by neuromodulators, since the system is on the boundaries of these phases. This raises the question of the likelihood of critical rhythmogenesis: what is the probability that a biological system will "choose" the exact rhythmic activity that also characterizes the bifurcation? One possible explanation is that the opposite took place. In other words, biological systems have evolved to operate at the critical conditions chosen by the critical rhythmogenesis mechanism. Thus, in our example, the characteristic delays, d, do not miraculously fit the desired rhythm. Rather, due to the specific values of d, the critical rhythmogenesis tunes the system to oscillate at ω_d, which is why the biological system "uses" this specific frequency band.

In our work, we made several simplifying assumptions to facilitate the analysis. We studied the dynamics of the effective couplings between excitatory and inhibitory populations and did not incorporate the STDP dynamics of individual

synapses. We investigated a model with only interconnections, hence ignoring the effective couplings that represent the intrapopulation synapses. We estimated neuronal correlations using a simplified rate model, and we did not study the effects of spiking neurons. These issues are beyond the scope of the current study and will be addressed elsewhere. Nevertheless, this work lays the foundation for studying a mechanism for robust homeostatic plasticity in general, and rhythmogenesis in particular.

ACKNOWLEDGMENT

This work was supported by the Israel Science Foundation, Grant No. 300/16.

APPENDIX: DETAILS OF THE NUMERICAL SIMULATIONS

1. STDP dynamics at finite λ

The STDP dynamics of the synaptic weights, J_E and J_I, at finite λ, Eq. (4), has been computed numerically. Using the separation of timescales, we solved the firing rate dynamics, Eqs. (7) and (8), for time intervals of $40\tau_m$ with fixed values of J_E and J_I, yielding the temporal evolution of $m_E(t)$ and $m_I(t)$ during that interval. We then generated spike trains approximating the inhomogeneous Poisson process in the following manner. The time interval of $40\tau_m$ was divided into time bins of $\Delta t = 0.001\tau_m$ (specifically, we used $\tau_m = 1$). In each time bin, the existence of a single spike was chosen in an independent manner following Bernoulli statistics with mean $m_X(t)\Delta t$, where $X \in \{E, I\}$. These spike times and the spike times of the previous interval were then used to update the synaptic weights using Eq. (4). This procedure was then repeated with the updated weights.

2. STDP dynamics with suppression of potentiation

The temporal evolution of the synaptic weights, J_E and J_I, was computed following the procedure described in Appendix 1. However, the potentiation term in Eq. (1) for J_E has been modified to

$$\Delta J_E = \lambda[f(J_E)K_+(\Delta) - \alpha K_-(\Delta)], \tag{A1}$$

where $f(J_E) = (1 - J_E/J_{E,\max})^\mu$ is the term that limits the potentiation for strong excitatory synapses. This change has modified the synaptic dynamics of Eq. (4) for the temporally asymmetric anti-Hebbian rule ($H = -1$) to

$$\dot{J}_E(t) = \lambda\left[f(J_E(t))\rho_E(t)\int_0^\infty \rho_I(t-t')K_+(-t')dt' - \alpha\rho_I(t)\int_0^\infty \rho_E(t-t')K_-(t')dt'\right]. \tag{A2}$$

The dynamics of J_I remained unchanged. Specifically, in Fig. 5(b) we used $\mu = 0.015$ and $J_{E,\max} = 7$.

3. STDP dynamics with a smooth transfer function

We replaced the threshold-linear transfer function, $[z]_+$, in Eqs. (7) and (8) with a smooth transfer function

$$\Phi(z) = \frac{z}{1 + e^{-bz}}. \tag{A3}$$

As the neuronal activity, $m_E(t)$ and $m_I(t)$, can now become negative, STDP dynamics cannot be computed using simulated spike times. Instead, we solved numerically the "mean-field" dynamics, Eq. (5), that is driven by the cross-correlations of the neuronal responses. The cross-correlations of the neuronal responses were computed by the temporal average of the product of their activities. The neuronal dynamics, Eqs. (7) and (8), has been solved for time intervals of $500\tau_m$ with time bins of $\Delta t = 0.001\tau_m$. Specifically, in Fig. 5(c) we used $\lambda_E = 10 \times \lambda_I = 0.004$, $b = 30$, and $I = 10$. We also used the suppression of strong excitatory potentiation, Eq. (A1), with $\mu = 0.015$ and $J_{E,\max} = 7$.

[1] R. Jung and W. Berger, Fiftieth anniversary of Hans Berger's publication of the electroencephalogram, His first records in 1924–1931 (author's translation), Arch. Psych. Nervenkrankheiten **227**, 279 (1979).

[2] G. Buzsáki, *Rhythms of the Brain* (Oxford University Press, Oxford, 2006).

[3] G. Buzsáki and W. Freeman, Editorial overview: brain rhythms and dynamic coordination, Curr. Opin. Neurobiol. **31**, v (2015).

[4] M. Bocchio, S. Nabavi, and M. Capogna, Synaptic plasticity, engrams, and network oscillations in amygdala circuits for storage and retrieval of emotional memories, Neuron **94**, 731 (2017).

[5] M. Shamir, O. Ghitza, S. Epstein, and N. Kopell, Representation of time-varying stimuli by a network exhibiting oscillations on a faster time scale, PLoS Comput. Biol. **5**, e1000370 (2009).

[6] A. H. Taub, R. Perets, E. Kahana, and R. Paz, Oscillations synchronize amygdala-to-prefrontal primate circuits during aversive learning, Neuron **97**, 291 (2018).

[7] C. M. Gray, P. König, A. K. Engel, and W. Singer, Oscillatory responses in cat visual cortex exhibit inter-columnar synchronization which reflects global stimulus properties, Nature (London) **338**, 334 (1989).

[8] P. Fries, J. H. Reynolds, A. E. Rorie, and R. Desimone, Modulation of oscillatory neuronal synchronization by selective visual attention, Science **291**, 1560 (2001).

[9] N. P. Bichot, A. F. Rossi, and R. Desimone, Parallel and serial neural mechanisms for visual search in macaque area v4, Science **308**, 529 (2005).

[10] B. Pesaran, J. S. Pezaris, M. Sahani, P. P. Mitra, and R. A. Andersen, Temporal structure in neuronal activity during working memory in macaque parietal cortex, Nat. Neurosci. **5**, 805 (2002).

[11] R. T. Canolty, E. Edwards, S. S. Dalal, M. Soltani, S. S. Nagarajan, H. E. Kirsch, M. S. Berger, N. M. Barbaro, and R. T. Knight, High gamma power is phase-locked to theta oscillations in human neocortex, Science **313**, 1626 (2006).

[12] A. J. Mably and L. L. Colgin, Gamma oscillations in cognitive disorders, Curr. Opin. Neurobiol. **52**, 182 (2018).
[13] W. Cao, S. Lin, Q.-q. Xia, Y.-l. Du, Q. Yang, M.-y. Zhang, Y.-q. Lu, J. Xu, S.-m. Duan, J. Xia *et al.*, Gamma oscillation dysfunction in mpfc leads to social deficits in neuroligin 3 R451C knockin mice, Neuron **97**, 1253 (2018).
[14] S. Ghosh, T. Rao Laxmi, and S. Chattarji, Functional connectivity from the amygdala to the hippocampus grows stronger after stress, J. Neurosci. **33**, 7234 (2013).
[15] P. J. Uhlhaas and W. Singer, Neural synchrony in brain disorders: relevance for cognitive dysfunctions and pathophysiology, Neuron **52**, 155 (2006).
[16] P. Fries, D. Nikolić, and W. Singer, The gamma cycle, Trends Neurosci. **30**, 309 (2007).
[17] A. Amir, D. B. Headley, S.-C. Lee, D. Haufler, and D. Pare, Vigilance-associated gamma oscillations coordinate the ensemble activity of basolateral amygdala neurons, Neuron **97**, 656 (2018).
[18] C. G. Welle and D. Contreras, New light on gamma oscillations, Neuron **93**, 247 (2017).
[19] T. Womelsdorf, P. Fries, P. P. Mitra, and R. Desimone, Gamma-band synchronization in visual cortex predicts speed of change detection, Nature (London) **439**, 733 (2006).
[20] Y. Luz and M. Shamir, Oscillations via spike-timing dependent plasticity in a feed-forward model, PLoS Comput. Biol. **12**, e1004878 (2016).
[21] A. Roxin, N. Brunel, and D. Hansel, Rate models with delays and the dynamics of large networks of spiking neurons, Prog. Theor. Phys. Suppl. **161**, 68 (2006).
[22] D. Battaglia, N. Brunel, and D. Hansel, Temporal Decorrelation of Collective Oscillations in Neural Networks with Local Inhibition and Long-Range Excitation, Phys. Rev. Lett. **99**, 238106 (2007).
[23] D. Battaglia and D. Hansel, Synchronous chaos and broad band gamma rhythm in a minimal multi-layer model of primary visual cortex, PLoS Comput. Biol. **7**, e1002176 (2011).
[24] A. Roxin and E. Montbrió, How effective delays shape oscillatory dynamics in neuronal networks, Physica D **240**, 323 (2011).
[25] S. Soloduchin and M. Shamir, Rhythmogenesis evolves as a consequence of long-term plasticity of inhibitory synapses, Sci. Rep. **8**, 13050 (2018).
[26] M. Shamir, Theories of rhythmogenesis, Curr. Opin. Neurobiol. **58**, 70 (2019).
[27] H. Câteau and T. Fukai, A stochastic method to predict the consequence of arbitrary forms of spike-timing-dependent plasticity, Neural Comput. **15**, 597 (2003).
[28] R. Gütig, R. Aharonov, S. Rotter, and H. Sompolinsky, Learning input correlations through nonlinear temporally asymmetric hebbian plasticity, J. Neurosci. **23**, 3697 (2003).
[29] A. Morrison, M. Diesmann, and W. Gerstner, Phenomenological models of synaptic plasticity based on spike timing, Biol. Cybern. **98**, 459 (2008).
[30] J. Rubin, D. D. Lee, and H. Sompolinsky, Equilibrium Properties of Temporally Asymmetric Hebbian Plasticity, Phys. Rev. Lett. **86**, 364 (2001).
[31] S. Song and L. F. Abbott, Cortical development and remapping through spike timing-dependent plasticity, Neuron **32**, 339 (2001).
[32] Y. Luz and M. Shamir, The effect of stdp temporal kernel structure on the learning dynamics of single excitatory and inhibitory synapses, PloS One **9**, e101109 (2014).
[33] G.-q. Bi and M.-m. Poo, Synaptic modifications in cultured hippocampal neurons: dependence on spike timing, synaptic strength, and postsynaptic cell type, J. Neurosci. **18**, 10464 (1998).
[34] M. A. Woodin, K. Ganguly, and M.-m. Poo, Coincident pre-and postsynaptic activity modifies gabaergic synapses by postsynaptic changes in cl- transporter activity, Neuron **39**, 807 (2003).
[35] A. Suvrathan, H. L. Payne, and J. L. Raymond, Timing rules for synaptic plasticity matched to behavioral function, Neuron **92**, 959 (2016).
[36] J. S. Haas, T. Nowotny, and H. D. I. Abarbanel, Spike-timing-dependent plasticity of inhibitory synapses in the entorhinal cortex, J. Neurophysiol. **96**, 3305 (2006).
[37] C. C. Bell, V. Z. Han, Y. Sugawara, and K. Grant, Synaptic plasticity in a cerebellum-like structure depends on temporal order, Nature (London) **387**, 278 (1997).
[38] M. Nishiyama, K. Hong, K. Mikoshiba, M.-M. Poo, and K. Kato, Calcium stores regulate the polarity and input specificity of synaptic modification, Nature (London) **408**, 584 (2000).
[39] R. C. Froemke, M.-m. Poo, and Y. Dan, Spike-timing-dependent synaptic plasticity depends on dendritic location, Nature (London) **434**, 221 (2005).
[40] T. Tzounopoulos, M. E. Rubio, J. E. Keen, and L. O. Trussell, Coactivation of pre-and postsynaptic signaling mechanisms determines cell-specific spike-timing-dependent plasticity, Neuron **54**, 291 (2007).
[41] D. O. Hebb, *The Organization of Behavior; A Neuropsychological Theory* (Wiley, New York, 1961).
[42] N. Sherf and S. Maoz, Multiplexing rhythmic information by spike timing dependent plasticity, PLoS Comput. Biol. **16**, e1008000 (2020).
[43] H. Câteau, K. Kitano, and T. Fukai, Interplay between a phase response curve and spike-timing-dependent plasticity leading to wireless clustering, Phys. Rev. E **77**, 051909 (2008).
[44] W. Gerstner, R. Kempter, J. Leo Van Hemmen, and H. Wagner, A neuronal learning rule for sub-millisecond temporal coding, Nature (London) **383**, 76 (1996).
[45] M. Gilson, M. Bürck, A. N. Burkitt, and J. Leo van Hemmen, Frequency selectivity emerging from spike-timing-dependent plasticity, Neural Comput. **24**, 2251 (2012).
[46] J. Karbowski and G. B. Ermentrout, Synchrony arising from a balanced synaptic plasticity in a network of heterogeneous neural oscillators, Phys. Rev. E **65**, 031902 (2002).
[47] R. R. Kerr, A. N. Burkitt, D. A. Thomas, M. Gilson, and D. B. Grayden, Delay selection by spike-timing-dependent plasticity in recurrent networks of spiking neurons receiving oscillatory inputs, PLoS Comput. Biol. **9**, e1002897 (2013).
[48] S. Lee, K. Sen, and N. Kopell, Cortical gamma rhythms modulate nmdar-mediated spike timing dependent plasticity in a biophysical model, PLoS Comput. Biol. **5**, e1000602 (2009).
[49] T. Masquelier, E. Hugues, G. Deco, and S. J. Thorpe, Oscillations, phase-of-firing coding, and spike timing-dependent plasticity: an efficient learning scheme, J. Neurosci. **29**, 13484 (2009).

[50] L. E. Muller, R. Brette, and B. Gutkin, Spike-timing dependent plasticity and feed-forward input oscillations produce precise and invariant spike phase-locking, Front. Comput. Neurosci. **5**, 45 (2011).

[51] J.-P. Pfister and P. Tass, Stdp in oscillatory recurrent networks: theoretical conditions for desynchronization and applications to deep brain stimulation, Front. Comput. Neurosci. **4**, 22 (2010).

[52] E. Aksay, I. Olasagasti, B. D. Mensh, R. Baker, M. S. Goldman, and D. W. Tank, Functional dissection of circuitry in a neural integrator, Nat. Neurosci. **10**, 494 (2007).

[53] J. Kim, M. Pignatelli, S. Xu, S. Itohara, and S. Tonegawa, Antagonistic negative and positive neurons of the basolateral amygdala, Nat. Neurosci. **19**, 1636 (2016).

[54] M. Koyama and A. Pujala, Mutual inhibition of lateral inhibition: a network motif for an elementary computation in the brain, Curr. Opin. Neurobiol. **49**, 69 (2018).

[55] D. Z. Jin and H. Sebastian Seung, Fast computation with spikes in a recurrent neural network, Phys. Rev. E **65**, 051922 (2002).

[56] T. Fukai and S. Tanaka, A simple neural network exhibiting selective activation of neuronal ensembles: from winner-take-all to winners-share-all, Neural Comput. **9**, 77 (1997).

[57] M. Shamir, The scaling of winner-takes-all accuracy with population size, Neural Comput. **18**, 2719 (2006).

[58] J. Hertz, A. Krogh, R. G. Palmer, and H. Horner, Introduction to the theory of neural computation, Phys. Today **44**(12), 70 (1991).

[59] M. Bazhenov, R. Huerta, and B. H. Smith, A computational framework for understanding decision making through integration of basic learning rules, J. Neurosci. **33**, 5686 (2013).

[60] C. K. Machens, R. Romo, and C. D. Brody, Flexible control of mutual inhibition: a neural model of two-interval discrimination, Science **307**, 1121 (2005).

[61] O. Zohar and M. Shamir, A readout mechanism for latency codes, Front. Comput. Neurosci. **10**, 107 (2016).

[62] S. M. Danner, N. A. Shevtsova, A. Frigon, and I. A. Rybak, Computational modeling of spinal circuits controlling limb coordination and gaits in quadrupeds, Elife **6**, e31050 (2017).

[63] J. Ausborn, A. C. Snyder, N. A. Shevtsova, I. A. Rybak, and J. E. Rubin, State-dependent rhythmogenesis and frequency control in a half-center locomotor cpg, J. Neurophysiol. **119**, 96 (2018).

[64] Y. Luz and M. Shamir, Balancing feed-forward excitation and inhibition via hebbian inhibitory synaptic plasticity, PLoS Comput. Biol. **8**, e1002334 (2012).

[65] G. Pernelle, W. Nicola, and C. Clopath, Gap junction plasticity as a mechanism to regulate network-wide oscillations, PLoS Comput. Biol. **14**, e1006025 (2018).

[66] O. Kinouchi and M. Copelli, Optimal dynamical range of excitable networks at criticality, Nat. Phys. **2**, 348 (2006).

[67] W. L. Shew, H. Yang, S. Yu, R. Roy, and D. Plenz, Information capacity and transmission are maximized in balanced cortical networks with neuronal avalanches, J. Neurosci. **31**, 55 (2011).

[68] O. Shriki and D. Yellin, Optimal information representation and criticality in an adaptive sensory recurrent neuronal network, PLoS Comput. Biol. **12**, e1004698 (2016).